

On modelling airborne infection risk

Yannis Drossinos^{1,*} and Nikolaos I. Stilianakis^{2,3,†}

¹*Thermal Hydraulics & Multiphase Flow Laboratory,
Institute of Nuclear & Radiological Sciences and Technology and Technology, Energy & Safety,
National Centre for Scientific Research “Demokritos”, 15314 Agia Paraskevi, Greece*

²*Joint Research Centre (JRC), European Commission, 21027 Ispra (VA), Italy*

³*Department of Biometry and Epidemiology, University of Erlangen-Nuremberg, Erlangen, Germany*

(Dated: December 25, 2023)

Airborne infection risk analysis is usually performed for enclosed spaces where susceptible individuals are exposed to infectious airborne respiratory droplets by inhalation. It is usually based on exponential, dose-response models of which a widely used variant is the Wells-Riley (WR) model. We revisit this infection-risk estimate and extend it to the population level. We use an epidemiological model where the mode of pathogen transmission, either airborne or contact, is explicitly considered. We illustrate the link between epidemiological models and the WR model. We argue that airborne infection quanta are, up to an overall density, airborne infectious respiratory droplets modified by a parameter that depends on biological properties of the pathogen, physical properties of the droplet, and behavioural parameters of the individual. We calculate the time-dependent risk to be infected during the epidemic for two scenarios. We show how the epidemic infection risk depends on the viral latent period and the event time, the time infection occurs. The infection risk follows the dynamics of the infected population. As the latency period decreases, infection risk increases. The longer a susceptible is present in the epidemic, the higher is its risk of infection by equal exposure time to the mode of transmission.

Keywords: infectious diseases, SARS-CoV-2 transmission, aerosol, airborne, infection risk, Wells-Riley infection risk model, Gammaitoni-Nucci infection risk model

I. INTRODUCTION

The determination of the risk of infection during an epidemic is an important quantitative indicator that, among others, influences decisions of public health authorities on intervention strategies and their implementation, including vaccine administration. It contributes, also, to individual decisions whether to accept recommendations of public health authorities on social distancing, proper wearing of face masks, and mobility restrictions. Estimates of the risk associated with airborne respiratory-pathogen infection have become numerous since the beginning of the coronavirus disease 2019 (COVID-19) pandemic.

Most airborne infection-risk analyses during the COVID-19 pandemic concentrated on risk calculations in small, enclosed spaces within which susceptible individuals are exposed to infectious airborne respiratory droplets by inhalation for a brief period. For example, the probability of infection due to the Severe Acute Respiratory Syndrome CoronaVirus 2, (SARS-CoV-2) has been estimated in numerous private and public micro-environments[1–7]. The majority of these risk analyses were based on the exponential, dose-response Wells-Riley (WR) model or its variants.

The Wells-Riley [8–10] model is a deterministic exposure model, based on the probabilistic airborne infection model proposed by Wells [11]. Wells introduced the quantum of airborne infection ¹ to be a discrete entity of the infectious dose that would, according to a Poisson distribution, give a 63.21% probability of infection [12] or, in modern terminology, the Infectious Dose ID_{63.21}. Riley et al. [8], expanding on Riley (1974) [13] and using Wells’ quantum of infection, introduced the average number of quanta inhaled during an individual’s exposure to an airborne pathogen in an exponential dose-response model. They, thus, proposed a model for the risk of airborne infection in an indoor environment. They assumed that the micro-environment is homogeneous, and hence infection quanta were uniformly distributed, and that the quantum concentration and the ventilation conditions were at steady state. The resulting steady-state model is commonly referred to as the Wells-Riley model. Moreover, they took I , the number of infectors, constant during exposure, but not so the number of susceptibles S , assuming that the viral latent period, the time between being infection and becoming infectious, is much longer than the exposure time, the duration individuals are exposed to the pathogen. An important generalisation of the WR model was proposed by Gammaitoni and Nucci

* email address: yannis.drossinos@gmail.com

† email address: nikolaos.stilianakis@ec.europa.eu; Corresponding author

¹ The choice of the word quantum refers to the discrete nature of the carriers of the airborne infection, i.e., the infectious respiratory droplets. Wells might have been paying homage to the great successes of quantum mechanics, universally accepted by the time he introduced the notion of a quantum of infection.

(GN) [14]. They removed the assumption of steady-state quantum concentration to generalise it to time-dependent quanta concentrations.

One of the characteristics of the WR model is that it uses input from aerosol dynamics to estimate viral transmissibility in, e.g., calculations of the generation rate of the quanta of infection, and their removal rate via e.g., gravitational settling or indoor-air ventilation. Human behaviour, however, is naively modeled by the lumped parameter of exposure time. The model, being an individual-level model and in contrast to compartmental epidemiological models, does not consider the total population N . Instead, the enclosed-space volume V determines the system scale.

Infection risk estimates in larger, including closed or semi-closed, populations and at longer, but intermediate, spatial and temporal time scales than those investigated by micro-environmental models are equally important. Envisioned intermediate spatial scales are those encountered in, e.g., hospitals, prisons, ships, nursing homes. Mesoscopic epidemiological models address these scales. The Susceptible-Infected-Recovered model with explicit modelling of the dynamics of the pathogen carrying agent (SIR-DC model [15, 16]) is one such model. The model considers that the pathogen-carrying agents, the pathogen “vector”, are either airborne infectious respiratory droplets (D) or deposited droplets (denoted by C, since the corresponding transmission mode is direct or indirect contact). In modelling the dynamics of the pathogen agent the SIR-DC model differs from the standard SIR model where the mode of pathogen transmission is only *implicitly* considered. Moreover, and contrary to micro-environmental models, the SIR-DC model is a population-level model.

Macroscopic models, on the other hand, address much larger populations and much longer temporal and spatial scales, for example country-wide and province scales [17–19] or regional scales [20]. At such scales, micro-environmental dynamics are not modeled. Instead, the intricate dynamics of respiratory droplets and other micro-environmental processes are implicitly incorporated via effective transmission rates or parameters, via a procedure akin to coarse-grained descriptions of physical systems [16].

Noakes et al. [10] presented an early attempt to reconcile the WR expression with a standard SIR compartmental epidemiological model. We use an extended version of the SIR-DC droplet model to revisit the derivation and to estimate what we shall refer to as the epidemic infection risk, the infection risk during an epidemic. We establish the connection between compartmental epidemiological models and micro-environmental risk models, like the Wells-Riley model and its Gammaitoni-Nucci generalisation, and the relevance of respiratory droplet dynamics. One of the essential observations is that neither the GN nor the WR model considers time-dependent changes of the infected population. In establishing this connection, we elucidate the meaning of the term *quantum of airborne infection*, introduced by William Firth Wells in his classic 1955 book [11]. As argued in Ref. [21], this term has been often confusingly interpreted.

Lastly, we calculate the epidemic infection risk, the probability to be infected, the event, at a specified time later than an arbitrarily chosen time during the epidemic. In essence, the question we address is: what is the probability at time t to be infected at a later time $t + \delta t$. The time t , with respect to the beginning of the epidemic, is the time at which risk is evaluated, and the time $t + \delta t$ is the event time. In our numerical simulations, we calculate this probability as a function of the pathogen latent period and as a function of the difference between the event time and the time the infection risk is calculated, δt , the risk time.

II. INFECTION PROBABILITY IN COMPARTMENTAL EPIDEMIOLOGICAL MODELS

The epidemic infection risk $P(t, \delta t; \langle \tau_{\text{exp}} \rangle)$, for an average daily exposure time $\langle \tau_{\text{exp}} \rangle$, is the probability at time t from the beginning of an epidemic to be infected at a future time $t + \delta t$ as specified by the event, i.e., the infection. The time difference δt is the time interval that determines how the infection risk at t depends on the evolution of the epidemic at $t + \delta t$. We shall refer to it as the risk time. The average daily exposure time is an estimate of a susceptible’s daily exposure to the pathogen: it is taken to be constant during an epidemic. For example, in the SIR-DC model the population dynamics depend on an average, daily exposure time which is embedded in the transmission rate (see Supplementary Material (SM)). In the standard SIR model the dynamics depend on the average exposure time implicitly via, e.g., the daily number of contacts between susceptible and infected individuals. As the average exposure time is taken to be constant, and the dependence of the probability on it is implicit, we shall simplify notation and refer to the infection probability as $P(t, \delta t)$ and the number of susceptibles as $S(t)$ (instead of $S(t; \langle \tau_{\text{exp}} \rangle)$).

The epidemic infection risk expressed in terms of the number of susceptible individuals S is their relative change [10, 22] in the period $[t, t + \delta t]$,

$$P(t, \delta t) = \frac{S(t) - S(t + \delta t)}{S(t)}. \quad (1)$$

Equation (1) provides the connection between epidemiological compartmental models and infection-risk models. Any

epidemiological model that calculates $S(t)$ can be used to calculate the probability of infection. In fact, the two approximation we will consider, WR and GN, refer to different approximate ways to calculate $S(t + \delta t)$.

The epidemic infection risk depends explicitly on two time scale ($t, \delta t$) and implicitly on $\langle \tau_{\text{exp}} \rangle$, in stark contrast to WR-based risk estimates that apparently depend on a single time scale, the time interval a susceptible is exposed to the pathogen. The time t , the time at which risk is calculated, may be additionally considered in WR-models as it determines the initial number of infectors. The risk time δt , i.e., difference between event and the time risk is evaluated, is analogous to the exposure time in WR-based model, in that it determines the interval over which the epidemiological populations evolve, and thus the time after t that the number of susceptibles $S(t)$ is to be determined. In the interval $[t, t + \delta t]$ the population $S(t)$ evolves according to model dynamics, herein taken to be the SIR-DC dynamics or the approximate dynamics the WR or GN models. In WR-like models the exposure time is the time over which the number of susceptibles changes, and thence the time scale that determines infection risk.

Another important difference between SIR-like and WR-based models is that the overall time scale of compartmental epidemiological models is of the order of days or months, whereas the time scale of WR-based risk analyses is of the order of hours.

III. SUSCEPTIBLE-EXPOSED-INFECTED-RECOVERED MODEL WITH TRANSMISSION MODES (SEIR-DC)

A. Droplet model

As other respiratory viruses, the SARS-CoV-2 virus exhibits a latent period. During the latent period $\tau_{\text{lat}} = 1/\sigma$ exposed individuals are infected but not infectious. Accordingly, we generalize the SIR-DC model of infectious disease transmission via infectious respiratory droplets [15] by adding an exposed population compartment E . The SIR-DC model is a population epidemiological model where individuals can move between the three standard epidemiological compartments of the SIR model. In addition, it models the dynamics of the pathogen carrying agent. Infection does not occur via direct $I \leftrightarrow S$ interaction: this interaction, instead, is mediated by the infectious droplets, be they airborne or settled.

A note is in order on the naming of the model. It was initially referred to as SDIR [16], a name that mixes epidemiological populations (S, I, R) with the pathogen-carrying agents (D, C) that determine the transmission mode. Stimulated by Ref. [23] and their SEIR-C model, we opted to separate epidemiological populations from transmission modes. Infectious respiratory droplet that are responsible for non-contact airborne transmission [24] are denoted by D (for droplets), whereas settled droplets that are responsible for contact transmission, direct or indirect, are denoted by C (for contact).

Bazant and Bush [25] also included the exposed population to connect the SEIR to the WR model. They, as we do herein, also considered cases of short and long latent periods of the pathogen. Our approaches differ, however, in how the epidemiological population compartments are coupled to the infectious respiratory droplets. The SEIR-DC model is defined by the following set of coupled ordinary differential equations (ODEs)

$$\frac{dS}{dt} = - \sum_{i=1}^{i=i_{\text{max}}} \left(\frac{\beta_i^d}{N} D_i S + \frac{\beta_i^c}{N} C_i S \right), \quad (2a)$$

$$\frac{dE}{dt} = -\frac{dS}{dt} - \sigma E, \quad (2b)$$

$$\frac{dI}{dt} = \sigma E - \mu_I I, \quad (2c)$$

$$\frac{dD_i}{dt} = \kappa_i^d I - \alpha_i^d D_i, \quad \text{for } i = 1, 2 \dots i_{\text{max}}, \quad (2d)$$

$$\frac{dC_i}{dt} = \kappa_i^c I - \alpha_i^c C_i, \quad \text{for } i = 1, 2 \dots i_{\text{max}}. \quad (2e)$$

We do not show the equation for the recovered compartment R since the total population $S + I + R = N$ is constant representing a closed population. A schematic diagram of the model is shown in Fig. 1.

The number of infectious airborne droplets of post-evaporation diameter d_i^{post} is denoted by D_i (number), and that of settled droplets by C_i (number), cf. SM for a discussion of droplet evaporation and associated droplet diameters. The number of droplet classes is i_{max} . The rate of transition from the exposed compartment E to the infected compartment I is denoted by σ . The infection recovery rate $I \rightarrow R$ is μ_I . Superscripts denote airborne droplet (d) and settled (c), and the subscript i denotes the droplet class specified by the post-evaporation diameter d_i^{post} . The

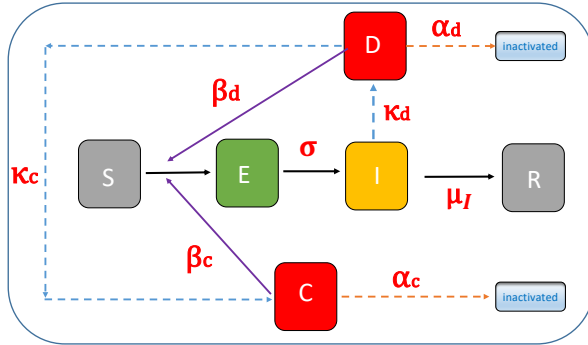


FIG. 1. Schematic diagram of the Susceptible-Exposed-Infected-Recovered model with transmission modes, SEIR-DC (based on a figure of Ref. [16]). Infectious droplet compartments are denoted by D_i , airborne droplets, and C_i , settled droplets. Superscripts (d, c) denote (airborne, settled) droplets, the subscript i refers to droplets with post evaporation diameter d_i^{post} . Infection transmission rates are denoted by $\beta_i^{d,c}$, droplet generation rates by $\kappa_i^{d,c}$, and removal rates by $\alpha_i^{d,c}$. The latent period is $\tau_{\text{lat}} = 1/\sigma$ and the infection recovery rate μ_I .

transmission rate per infectious, airborne respiratory droplet that has been inhaled and deposited in the respiratory tract of a susceptible is denoted by β_i^d (inverse time), whereas that of an infectious settled droplet transferred to facial membranes is denoted by β_i^c (inverse time).

The airborne droplet generation rate per infected individual (by normal oro-nasal activities-e.g., speaking, laughing, breathing- or by violent expiratory events - sneezing, coughing-) is κ_i^d (number/time) and the corresponding airborne droplet removal rate is α_i^d (number/time), the later including droplet removal by ventilation (if present). Settled droplets may be generated either via direct generation by an infected individual and deposition on facial mucous tissues or via deposition of airborne droplets. Direct deposition would introduce an additional generation term in Eq. (2e) proportional to the number of infected individuals, similar to the generation term in the airborne-droplet equation, Eq. (2d). In this version of the model we neglect this mechanism. Instead, settled droplets are generated via deposition of airborne droplets, and specifically solely by gravitational settling. Hence the generation rate $\kappa_i^c = \theta_i(d_i^{\text{post}})$ (number/time) with θ the gravitational settling rate in still air. The corresponding settled droplet removal rate is α_i^c (number/time).

We present expressions for the transmission $\beta_i^{c,d}$ and removal $\alpha_i^{c,d}$ rates, along with justifications for our choices, in SM. We remark that the transmission and removal rates are *derived* quantities. In addition, both transmission rates depend (linearly as we argue in SM) on the average exposure time $\langle \tau_{\text{exp}} \rangle$. The SIR-DC basic reproduction number is [15, 16]

$$R_0^{\text{SIR-DC}} = \sum_{i=1}^{i=i_{\text{max}}} \left(\frac{\beta_i^d \kappa_i^d}{\alpha_i^d \mu_I} + \frac{\beta_i^c \kappa_i^c}{\alpha_i^c \mu_I} \right). \quad (3)$$

Equation (3) also gives the SEIR-DC basic reproduction number, see, for example, Ref. [26].

B. Infectious quanta: Gammaitoni-Nucci approximation

We limit the droplet classes to a single airborne droplet class D_1 (SEIR-D) as the original GN model considered only one droplet diameter. It can be shown, for example by integrating the infected population Eq. (2c), that if $\sigma \delta t \ll 1$, latent period much greater than the risk time (the time the epidemiological populations evolve to calculate the infection probability), and $\mu_I \delta t \ll 1$, infectiousness period much greater than the risk time δt , then $dI/dt|_{t=t_0} = 0$. Hence, under these limits, the number of infected at time t , here taken to be the initial time t_0 , may be considered to be constant and denoted as I_0 . If, in addition, we disregard the equation for the exposed population Eq. (2b), which is irrelevant over the risk time δt for the time-development of the infection, $\sigma \delta t \ll 1$ (the number of E increases, but

not that of I), the SEIR-D model reduces to

$$\frac{dS}{dt} = -\frac{\beta_1^d}{N} D_1 S, \quad (4a)$$

$$\frac{dD_1}{dt} = \kappa_1^d I_0 - \alpha_1^d D_1. \quad (4b)$$

The system of Eqs. (4a,4b) can be compared to the GN equations (5) for the rate of change of the number of susceptibles and total number of quanta of infection Q in the enclosed space. The GN equations expressed in our notation read

$$\frac{dS}{dt} = -\frac{B}{V} Q S, \quad (5a)$$

$$\frac{dQ}{dt} = q I_0 - \lambda_{\text{air}} Q, \quad (5b)$$

where q is the quantum generation rate per infectious individual (quanta/sec), see also [10], B is the breathing rate (m^3/sec), and V is the space volume (m^3). The parameter λ_{air} is the quantum removal rate which in the initial formulation of the model was taken to be the ventilation rate in air exchanges per hour [14]. Since then, it has been expanded to include the rate of pathogen inactivation, droplet surface deposition, inactivation due to UV irradiation, filter penetration, mask efficiency, etc. (see also the droplet removal rates α_1^d used in this work and summarized in SM).

The analytical solution of Eq. (5b) is

$$Q(t) = \frac{q I_0}{\lambda_{\text{air}}} + \left(Q_0 - \frac{q I_0}{\lambda_{\text{air}}} \right) \exp(-\lambda_{\text{air}} \delta t), \quad (6)$$

where Q_0 is the initial (at time $t = t_0$) total concentration of the infection quanta in the enclosed space.

Even though the two sets of equations Eqs. (4) and (5) are formally equivalent, their interpretation and the time scales chosen to determine infection risk differ. In our numerical simulations we use typical time scales associated with compartmental epidemiological models, of the order of months. WR-based models in micro-environments, instead, use considerably shortened time scales, of the order of hours.

In Section IV, we use the GN equations to approximate the dynamics of the number of susceptibles $S(t)$, and subsequently the infection risk according to Eq. (1). As the droplet equation Eq. (4b), and subsequently the susceptible equation Eq. (4a), may be solved analytically, in our numerical simulations we used the analytical solutions.

1. What are infection quanta?

The comparison of Eqs. (4) and (5) provides insights on the differences and formal similarities of the SEIR-D and GN models. Let the number of quanta of infection be proportional to the number of infectious respiratory droplets

$$Q = \xi D_1, \quad (7)$$

and the transmission rate proportional to the breathing rate, $\beta_1^d = B \tilde{\beta}_1^d$, as argued in SM. Moreover, for the purposes of this comparison, consider indoor-air ventilation the only droplet or quantum removal process, $\alpha_1^d = \lambda_{\text{air}}$. Their substitution into Eqs. (4), and a mapping of the resulting equations to Eqs. (5) determines the conversion factor ξ to be

$$\xi = \frac{\beta_1^d}{B} \frac{V}{N} \equiv \tilde{\beta}_1^d \rho_{\text{scale}}, \quad (8)$$

where the last equation defines the scaling density $\rho_{\text{scale}} = V/N$. Hence, in this model infection quanta, up to an overall scaling density, are infectious respiratory droplets modified by $\tilde{\beta}_1^d$, a parameter that includes the probability of infection of a lung-deposited pathogen, number of pathogens in a droplet, lung-deposition probability, and average exposure time, cf. SM. The combination of these factors converts infectious airborne droplets to infection quanta. Their generation q is similarly related to the respiratory droplet generation rate via $q = \kappa_1^d \xi$.

The mapping of the two models also manifests the different inherent system scales: the extensive variable, namely the variable that scales linearly with the size of the system, is the volume of the enclosed space in the GN model, whereas it becomes the total population N in the SEIR-D model. The scaling density ρ_{scale} implements the transition

from a microscopic models, which depends on the enclosed-space volume V , to a mesoscopic epidemiological model, which depends on the total population N . This scaling is reminiscent of the scaling proposed in Ref. [17] to transition from an ODE to a PDE epidemiological model.

Care should be exercised in interpreting ρ_{scale} : if V is taken to refer to a mesoscopic volume, then the GN model is essentially extended to much greater scales. If N is taken to be the number of individuals in an enclosed, micro-environment the SIR-D model is restricted to smaller scales; however, in that case it may not be considered a proper compartmental epidemiological model. These consideration have important repercussion on the choice of model parameters and risk times in micro or mesoscale models.

C. Wells-Riley approximation

Reference [27] considered analytically the very common limit where the duration of infectiousness of an infected individual $T_I = 1/\mu_I$ is significantly longer than the lifespan of the airborne pathogen $T_p = 1/\alpha_1^d$, i.e., when $\rho_1 \equiv \mu_I/\alpha_1^d = T_p/T_I \ll 1$. For appropriately chosen non-dimensional variables [27] the quasi steady-state limit is defined as $\rho_1 d\tilde{D}_1/d\tilde{t} = 0$ which implies $\tilde{D}_{1,\text{qss}} = \tilde{I}$, or in terms of the original variables $D_{1,\text{qss}} = (\kappa_1^d/\alpha_1^d)I$. Note that the quasi steady-state condition does *not* imply that the number of infected individuals is constant, $dI/dt|_{\text{qss}} \neq 0$, that is I_{qss} is *time dependent*.

The substitution of the steady-state (I, D_1) relationship in the original equations Eqs. (2) gives the quasi steady-state limit of SEIR-D,

$$\frac{dS_{\text{qss}}}{dt} = -\frac{\beta_1^d \kappa_1^d}{\alpha_1^d N} I_{\text{qss}} S_{\text{qss}}, \quad (9a)$$

$$\frac{dE_{\text{qss}}}{dt} = \frac{\beta_1^d \kappa_1^d}{\alpha_1^d N} I_{\text{qss}} S_{\text{qss}} - \sigma E_{\text{qss}}, \quad (9b)$$

$$\frac{dI_{\text{qss}}}{dt} = \sigma E_{\text{qss}} - \mu_I I_{\text{qss}}. \quad (9c)$$

In the quasi steady-state limit the dependence on the number of infectious droplets $D_1(t)$ disappears.

As before, in the previously considered double limit, $\sigma\delta t, \mu_I\delta t \ll 1$, we can neglect the equation for the exposed population, Eq. (9b), and take the number of infected individuals constant, $I_{\text{qss}} = I_0$. The analytical solution of the resulting model leads directly to the WR approximation of the SEIR-D model

$$P_{\text{WR}}^{\text{SEIR-D}}(t, \delta t) = 1 - \exp\left(-\frac{\beta_1^d \kappa_1^d}{\alpha_1^d N} I_0 \delta t\right). \quad (10)$$

Hence, the WR equation is obtained from the quasi steady-state SEIR-D equations in the triple limit of latent period and infectiousness period longer than the time scale of observation and $\rho_1 \ll 1$. Substitution of $k_1^d = q/\xi$, along with Eq. (8), and $\alpha_1^d = \lambda_{\text{air}}$ in Eq. (10) leads to the WR infection probability as usually written.

Of course, the WR approximation to the GN model may be easily obtained by setting $dQ/dt = 0$ in Eq. (5b). The steady-state quantum concentration, then, becomes $Q_{\text{ss}} = qI_0/(\lambda_{\text{air}})$, leading via Eq. (5a) to the number of susceptibles and, thus, to the WR infection risk. However, the alternative derivation for the WR approximation we presented in terms of the quasi steady-state solution of the SEIR-D model specifies the region of validity of the approximation, instead of arbitrarily setting $dQ/dt = 0$.

IV. NUMERICAL RESULTS

We performed numerical simulations of the SEIR-D model, Eqs. (2), to investigate the effect of the event time $t + \delta t$, via δt , and of the latent period τ_{lat} on epidemic infection risk. As mentioned, we address the question of what is the probability at time t , any arbitrarily chosen time during the epidemic, to be infected at a future event time $t + \delta t$, given the evolution of the pandemic till $t + \delta t$. We also investigate numerically and analytically the validity of the GN, Eqs. (4), and WR, Eq. (10), approximations to the SIR-D population dynamics.

For the simulations we used parameters related to the COVID-19 pandemic, e.g., individual behaviour characteristics in addition to physico-chemical and biological properties of the SARS-CoV-2 virus. We note, though, that we do not attempt to reproduce a COVID-19 scenario as in our attempt to present the minimal model that reduces to the GN or WR models we do not consider the asymptomatic stage of the disease.

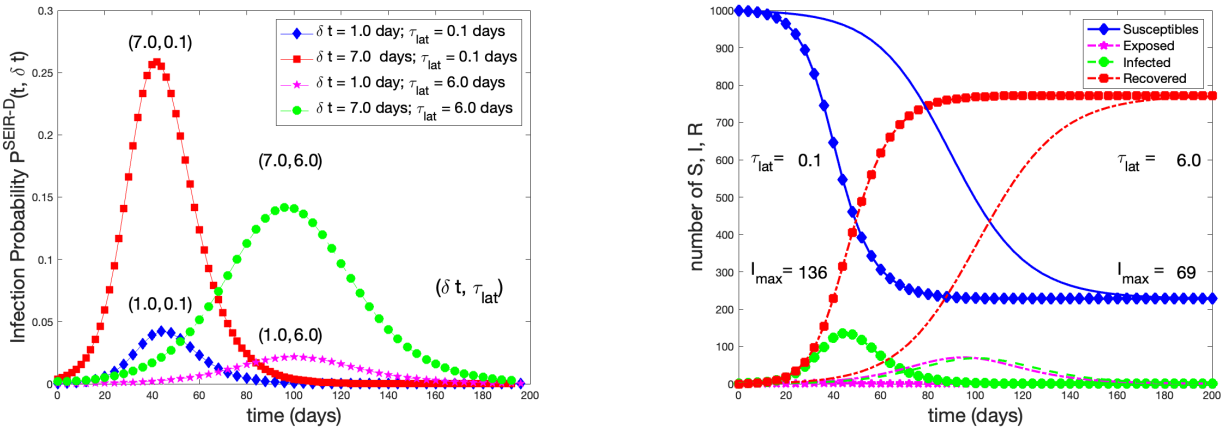


FIG. 2. Left: Epidemic infection probability, i.e., the probability at t to be infected at a future time $t + \delta t$, according to the SEIR-D model. Curves were calculated for two risk times ($\delta t = 1, 7$ days) and two latent periods ($\tau_{\text{lat}} = 0.1, 6$ days). Two airborne-droplet classes were considered, ($d_i^{\text{post}} = 2.05, 82.13 \mu\text{m}$ ($i = 1, 2$)), susceptible-infectious droplet encounters per day were taken to be $c = 18$, exposure time for each $S \leftrightarrow D_i$ ($i = 1, 2$), encounter $\tau_{d_1} = 25$ min and $\tau_{d_2} = 1$ min, leading to a total daily susceptible-infectious droplet average exposure time of $\langle \tau_{\text{exp}} \rangle = 7.8$ hours (per day). The ventilation rate was taken to be $\lambda_{\text{air}} = 0.2$ air exchanges per hour, a typical value for an Italian building [1]. Total population $N = 1000$. Right: Corresponding dynamics of the two epidemics. The left curves (filled symbols) correspond to the short latent period, $\tau_{\text{lat}} = 0.10$ days, with I peaking at $t \approx 43$ days, and no discernible exposed population. The right curves (lines, no symbols) show the epidemic for the long latent period $\tau_{\text{lat}} = 6$ days, with I peaking at $t \approx 96$ days, and an appreciable exposed population.

We used two airborne droplet classes of post-evaporation diameter $d_i^{\text{post}} = 2.05, 82.13 \mu\text{m}$ ($i = 1, 2$). As generally accepted [28], the pathogen concentration was taken to be droplet-size dependent. We opted to limit the airborne droplet classes to two and not to simulate settled droplets to render easier the interpretation of our results: either condition can be easily relaxed. The evaporation factor [16], $d_i^{\text{post}} = z_{\text{evap}} d_i^{\text{pre}}$, was set to $z_{\text{evap}} = 0.40$. Airborne droplet generation rates were taken to correspond to speaking. A complete list of model parameters is presented in SM.

Individual behaviour determines a number of model parameters. We considered the contact rate, the number of susceptible-infected individual encounters, to be $c = 18$ per day [29]. The exposure time of a susceptible with an infectious droplet, i.e., the breathing time during a $S \leftrightarrow I$ encounter, was taken to depend on the droplet size: $\tau_{d_1} = 25$ min and $\tau_{d_2} = 1$ min. Thus, the average exposure time per day of a single susceptible is $c \times (\tau_{d_1} + \tau_{d_2}) = 7.8$ hours per day.

Figure 2 summarizes the main results of four simulations to determine the probability at time t that infection occurs at the event time $t + \delta t$. We used two latent periods $\tau_{\text{lat}} = 0.1$ days (short) and $\tau_{\text{lat}} = 6.0$ days (long), along with a short $\delta t = 1.0$ day and a long relative time interval $\delta t = 7$ days. The left panel shows the calculated infection probabilities for each scenario. Two groups of curves may be identified: for the short latent period the infection probability peaks at about $t_{\text{peak}} \approx 43$ days, whereas for the long latent period the peak occurs at $t_{\text{peak}} \approx 96$. Within each group of curves, infection risk increases with increasing risk time.

The qualitative behaviour of infection risk may be understood by considering the dynamics of the epidemic, described by the time-dependent number of S, E, I and R shown in the right panel of Fig. 2. The four curves on the left (filled symbols) correspond to the short latent period, whereas those on the right (no symbols) to the long latent period. We also present the maximum number of infected individuals I_{max} for each epidemic. For the short-latent period epidemic, the number of exposed individuals is very small, not discernible on the figure, whereas for the long-latent period epidemic the number of exposed individuals is comparable to the number of infected. In fact, before the I maximum, $E > I$, whereas afterwards $I > E$. Even though not discernible, the number of exposed individuals E peaks earlier than the number of infected I .

We find that infection risk follows the time-dependent behaviour, the dynamics, of the infected individuals I . As the number of infected increases, infection risk increases, and vice versa. As the latency period decreases infection risk increases, since the number of infected increases. In addition, for the same pathogen (latent period constant) infection risk increases with increasing risk time δt , i.e., with increasing difference between event time and time t , the time risk is evaluated. In fact, this is a general result: the longer the epidemic evolves and the longer a susceptible is present in it, the more likely the individual is to be infected.

The validity of the GN and WR approximations to the SEIR-D dynamics is investigated numerically in Fig. 3. Four groups of curves are shown, each corresponding to the ordered pair $(\delta t, \tau_{\text{lat}})$. For each pair choice, we plot the SEIR-D infection risk calculated via the numerical solutions of Eqs. (2) (filled blue diamonds), infection risk calculated via the GN approximation and described in Section III B (square, unfilled symbols), and via the WR approximation $P_{\text{WR}}^{\text{SEIR-D}}$ as calculated via Eq. (10) (cross, continuous line).

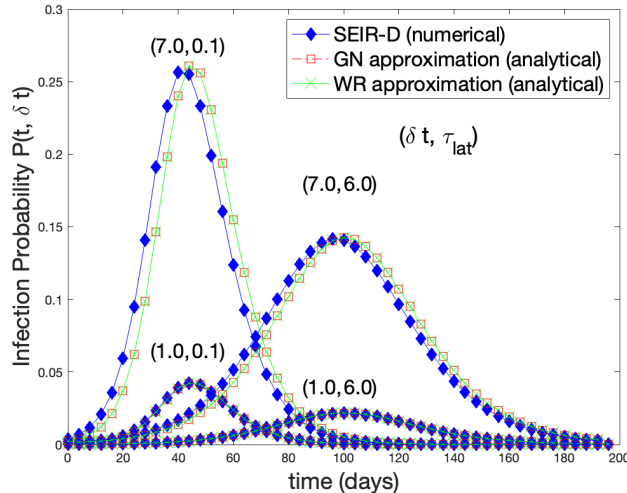


FIG. 3. Epidemic infection probability calculated via the SEIR-D model and its GN, and WR approximations, Eq. (10). The four ordered pairs associated with each graph triplet are specified by $(\delta t, \tau_{\text{lat}})$. For all the simulations the GN and WR limits were identical: they differed from the SEIR-D model predictions only for the long risk time ($\delta t = 7$ days). See the main text for the explanation.

Two observations are in order. For the epidemics considered, the GN and WR limits are identical. Whether the two limits would differ depends on the airborne droplet removal rate α_1^d (and hence on the dimensionless parameter $\rho_1 = \mu_I/\alpha_1^d$).² The importance of the removal rate is apparent from the analytical solution of the droplet equation Eq. (4b). Its time-dependent part, which is formally identical to the second term of Eq. (6), determines the difference between the steady-state and non steady-state model. It vanishes as $\alpha_1^d \delta t \gg 1$, a condition satisfied for all cases considered. The same observation holds for the GN-WR comparison. If ventilation is the dominant aerosol removal process, for $\lambda_{\text{air}} \delta t \gg 1$ the two models become identical. Hence, for high ventilation rates the difference between the steady and non steady-state quantum concentration models decreases or even vanishes.

The other observation is that for the short risk time $\delta t = 1$ day all three calculations predict the same infection risk, irrespective of the viral latent period. The calculated risks differ for the long risk time, the difference increasing with the latent period decreasing, i.e., as $\tau_{\text{lat}} \rightarrow 0$. For short latent periods the time dependence of the infected $I(t)$ can not be neglected. As the number of I increases, i.e., before the maximum of the number of infected, the GN and WR approximate dynamics underestimate infection risk, whereas the opposite holds when $dI/dt < 0$. This arises because when the number of I increases more infectious droplets are generated than predicted for a constant I_0 leading to a larger infection probability, and vice versa.

In an attempt to investigate the GN-WR difference we considered an extreme case of the SEIR-D model by shortening the model time scales from days to hours. The calculated infection risk, not shown, behaved as described in the previous paragraphs, confirming the initial observation that even for short risk times, e.g., $\delta t = 12$ hours, the condition $\alpha_1^d \delta t \gg 1$ remained valid. We note that the GN and WR models may, however, differ in micro-environmental simulations if the necessary condition, e.g., $\alpha_1^d \delta t \ll 1$ are satisfied.

² We restrict the analysis to a single airborne droplet class, for simplicity: the arguments are easily generalized.

V. DISCUSSION

We presented a model to calculate epidemic infection risk, namely the probability that at an arbitrarily chosen time t during the epidemic infection occurs at a future event time $t + \delta t$. The SEIR-DC model consists of the standard epidemiological populations of the Susceptible-Exposed-Infected-Recovered (SIR) populations coupled to the dynamics of the pathogen-carrying agent, and hence to the pathogen transmission mode. The pathogen-carrying agent is taken to be either airborne infectious respiratory droplets (D), as in the case of airborne infections such as COVID-19 or influenza, or settled droplets responsible for (direct or indirect) contact transmission (C). The model provides a connection between SEIR-like epidemiological models and infection-risk models based on Wells-Riley [8] models, including the non-steady state generalisation proposed by Gammaitoni and Nucci (GN) [14]. In fact, the SEIR-DC model may be viewed as a generalisation of the GN model to the population level for arbitrary viral latent periods. We emphasized the importance of system scales, since both the GN and WR models are individual-level models that describe infection risk in enclosed micro-environments. SEIR-like models instead are population-level models.

We argued that for long latent periods of the pathogen the SEIR-DC model reduces to a set of equations that are reminiscent of the GN equations. Their mapping identified infection quanta as infectious respiratory particles modified by a scaling density and, more importantly, by a combination of parameters that include biological properties of the pathogen (size-dependent pathogen droplet concentration, probability of infection due to a deposited infectious droplet), physical properties (lung-deposition probability), and behavioural properties (exposure time). We noted that the SEIR-DC epidemiological model depends on the total population N , whereas both the WR and GN models consider much smaller scales in terms of the enclosed volume V . We identified the scaling density as the factor to transition from one class of models to the other, and we discussed how this density allows a generalisation of micro-environmental models.

We performed numerical simulations of two scenarios for an epidemic specified by a short and a long latent period and driven by two classes of airborne infectious droplets. Model parameter were based on properties of the SARS-CoV-2 virus, even though we do not claim to model specifically the SARS-CoV-2 transmission dynamics with all of their characteristics. However, the SARS-CoV-2 transmission dynamics reflect those of a range of airborne infections such as influenza.

Our numerical simulations determine the risk at any time t to be infected at a future event time $t + \delta t$, as determined from the evolution of the epidemic in the time interval $[t, t + \delta t]$. We were particularly interested in the dependence of the calculated infection probability on the event time $t + \delta t$ via δt . We found that infection risk follows the dynamics of the infected population: as the number of infected increases so does the risk, and vice versa. As the latency period decreases, infection risk increase. Moreover, as the difference between the event and the time at which risk is evaluated increases, i.e., as the risk time increases, infection risk increases. Equivalently, the longer the epidemic evolves, the longer an individual is present in an epidemic, the more likely that the individual gets infected, and hence infection risk increases.

The WR and GN approximations of the SEIR-D dynamics reproduced accurately calculated infection risk. Differences arose for large time intervals δt ($\delta t = 7$ days), increasing with decreasing viral latent period. We remarked that the WR and GN approximate forms of the epidemic infection risk were almost identical for all our simulations. This arises when the droplet removal rate α_1^d is much greater than the inverse risk time, i.e., $\alpha_1^d \delta t \gg 1$. In fact, this is a general result suggesting that with increasing droplet removal rates, for example via increased ventilation rate, the WR-calculated airborne infection risk with a steady-state quantum concentration provides an excellent approximation to the GN-calculated infection risk with non-steady-state quantum concentrations.

The comparative analysis presented here bridges the gap and provides the missing links in the mathematical relationship between individual infection risk models and associated population based models. The corresponding insights allow for a more nuanced epidemiological interpretation of infectious disease outbreaks.

ACKNOWLEDGMENTS

YD would like to thank the PEACoG (Physical Epidemiology Amherst Covid Group) members for their many insightful discussions and helpful comments over the last years. We thank Marguerite Robinson for discussions during the initial stages of our work, and Vladimir M. Veliov for comments on the connection between the SIR-D and WR models. The views expressed are purely those of the authors and may not in any circumstances be regarded as stating an official position of the European Commission.

DATA AVAILABILITY STATEMENT

The study has no original data. The numerical results of this study are available within this paper. The parameter values and their justification are in the Electronic Supplementary Material of this paper.

AUTHOR CONTRIBUTIONS

Y.D. designed research, performed research, analyzed the results and wrote the article; N.I.S. designed research, analyzed the results, and wrote the article.

COMPETING INTEREST

The authors declare no competing interest

FUNDING

The research was performed with institutional support only.

Appendix A: Supplementary Material

1. Susceptible-Exposed-Infected-Recovered with transmission modes (SEIR-DC): Model parameters

The droplet population compartments D_i , number of airborne droplets, and C_i , number of settled droplets, are identified by the droplet diameter. Respiratory droplets are generated in the respiratory tract under conditions of 100% relative humidity and approximately 37° C degrees. Upon expulsion, they equilibrate quickly to the local temperature and relative humidity conditions by water evaporation. As evaporation is a molecular process, droplet shrinking occurs very rapidly, see, for example Refs. [24, 30–32], and the droplet diameter after equilibration is the droplet diameter most often experimentally accessible. We refer to the droplet diameter at generation as the pre-evaporation diameter, d_i^{pre} , and that after equilibration as the post-evaporation diameter, d_i^{post} . Their ratio defines the evaporation factor [16] ζ_{evap}

$$d_i^{\text{post}} = \zeta_{\text{evap}} d_i^{\text{pre}}. \quad (\text{A1})$$

The pre-evaporation diameter, via ρ_p the pathogen concentration at the location of droplet generation, e.g., oral region, determines the number of pathogens $N_{\text{path}}^{(i)}$, within a d_i^{pre} droplet,

$$N_{\text{path}}^{(i)} = \rho_p(d_i^{\text{pre}}) \times \frac{\pi}{6} (d_i^{\text{pre}})^3 = \rho_p(d_i^{\text{pre}}) \times \frac{\pi}{6} (d_i^{\text{post}}/\zeta_{\text{evap}})^3. \quad (\text{A2})$$

The post-evaporation diameter determines the physical properties of the droplet like the removal rate λ_{dep} , via gravitational settling or other surface-deposition processes, and droplet transport processes. We also consider that it determines their lung-deposition probability q_{d_i} . These observation confirm the importance of the evaporation factor ζ_{evap} , a factor that depends strongly on the ambient relative humidity. Not only does it determine $N_{\text{path}}^{(i)}$ and the droplet deposition and transport properties, it also influences viral infectivity, and eventually the viral inactivation rate $\mu_{d,c}$ in that changes in the droplet diameter lead to changes of the concentration of the within-droplet species [16]. These concentration changes may have important consequences since, for example, increased concentration of salts, proteins, organics, and acid may damage the pathogen and modify its infectivity [33, 34].

a. Transmission rates

The infection transmission rates depend on numerous parameters that may be categorised as biological, behavioral, or physical. In Ref. [15] we showed that the transmission rate associated with a d_i^{post} droplet, be it airborne β_i^d or settled β_i^c , may be expressed as

$$\beta_i^d = c\tau_{d_i} \times \frac{B}{V_{cl}} q_{d_i} \times p_d \times \rho_p^{(i)}(d_i) \times \frac{\pi}{6} (d_i^{\text{post}}/\zeta_{\text{evap}})^3 \times \epsilon_i^d, \quad i = 1, \dots, i_{\text{max}}, \quad \text{airborne droplets}, \quad (\text{A3a})$$

$$\beta_i^c = c\tau_{c_i} \times \eta_c q_{c_i} \times p_c \times \rho_p^{(i)}(d_i) \times \frac{\pi}{6} (d_i^{\text{post}}/\zeta_{\text{evap}})^3 \times \epsilon_i^c, \quad i = 1, \dots, i_{\text{max}}, \quad \text{settled droplets}, \quad (\text{A3b})$$

where i_{max} is the total number of droplet compartments as specified by their post-evaporation diameter. In the main text, we also argued that the breathing rate B (m^3/day) may be factored out in Eq. (A3a) to define

$$\tilde{\beta}_i^d \equiv \frac{\beta_i^d}{B} = c\tau_{d_i} \times \frac{1}{V_{cl}} q_{d_i} \times p_d \times \rho_p^{(i)}(d_i) \times \frac{\pi}{6} (d_i^{\text{post}}/\zeta_{\text{evap}})^3 \times \epsilon_i^d, \quad (\text{A4})$$

a parameter that converts infectious respiratory droplets to infection quanta.

The parameters in Eqs. (A3) that depend on biological properties are: the pathogen concentration $\rho_p^{(i)}$ at the generation location of droplet d_i^{pre} (number per volume) which we take to be droplet-size dependent; the probability of infection p_d due to a lung-deposited airborne droplet per pathogen (dimensionless); and the probability of infection p_c due to a settled droplet that has been transferred from a surface to a susceptible individual facial membranes per pathogen. The breathing rate B may also be consider a biological parameter, but we prefer to consider it a physical parameter (see Table I). Lastly, the infection recovery rate μ_I (number per day), not present in Eqs. (A3), is also a biologically-determined parameter.

We consider the lung-deposition probability q_{d_i} of a d_i^{post} droplet to be a physically determined parameter. The characteristic personal-cloud volume, the volume surrounding an individual, is denoted by V_{cl} . Recently, Xenakis

(2023) [35] referred to the personal-cloud volume as the “breathing zone volume, i.e., the air volume surrounding a susceptible occupant and determining their epidemiological status”.

The transmission-rate parameters that depend on an individual’s behavior include the individual-infectious person average contact rate c (number per day), and the transfer rate of settled droplets to facial mucus membranes η_c (number per day). During each infectious-susceptible encounter, the susceptible individual is exposed to airborne infectious droplets for a droplet-depending breathing time τ_{d_i} (days), and to settled infectious droplets for the duration of a hands-face exposure time τ_{c_i} (days). The combination of these average exposure times per contact leads to an average total exposure time to infectious droplets per day of $\langle \tau_{\text{exp}} \rangle = c \times \sum_i^{i_{\text{max}}} (\tau_{d_i} + \tau_{c_i})$.

The parameters $\epsilon_i^{d,c}$ include other effects that could modify the transmission rates and not initially considered in Ref. [15]. For example, the filtration efficiency of personal protective equipment or face masks is an important factor that should be included in ϵ_i^d .

b. Removal rates

The droplet removal rates are *effective* removal rates of infectious droplets in that they include virus inactivation in addition to more traditional removal rates like surface deposition or removal induced by indoor air ventilation. The removal rates of airborne α_i^d and settled α_i^c droplets of post-evaporation diameter d_i^{post} are

$$\alpha_i^d = (1 + c\tau_{d_i}) \frac{B}{V_{cl}} q_{d_i} + \mu_d + \lambda_{\text{dep}}^i(d_i^{\text{post}}) + \lambda_{\text{air}} + \phi_i^d, \quad i = 1, \dots, i_{\text{max}}, \quad \text{airborne droplets}, \quad (\text{A5})$$

$$\alpha_i^c = (1 + c\tau_{c_i}) \eta_c q_{c_i} + \mu_c + \phi_i^c, \quad i = 1, \dots, i_{\text{max}}, \quad \text{settled droplets}. \quad (\text{A6})$$

Similarly to the infection transmission rates, droplet removal mechanisms may be associated with behavioural, biological, or physical processes. The first term in both Eq. (A5) and (A6) is a self removal term: in the case of airborne droplets it models removal by inhalation by the susceptible (shown to be negligible for influenza-related parameters [36]), in the case of settled droplets is self-transfer of a deposited droplet to facial membranes. The viral inactivation rate in airborne droplets is denoted by μ_d (number per day), and that of settled droplets by μ_c (number per day). They are determined by the properties of the virus under ambient conditions, and hence a strong function of the relative humidity [16]. The ventilation rate is denoted by λ_{air} (number of air exchanges per day), whereas the surface deposition rate is denoted by λ_{dep} (number of droplets per day.) In our simulations we considered that the only physical processes that leads to droplet deposition is gravitational settling, $\lambda_{\text{dep}}^i = \theta(d_i^{\text{post}})$.

The parameters $\phi_i^{d,c}$ denote any other process that might induce particle removal: for example, UV radiation would be an additional viral inactivation mechanism that would modify $\mu_{d,c}$. Another possible inactivation mechanism would be indoor spraying of nonhazardous levels of an acid, e.g., nitric, to decrease droplet pH [33] or spraying a basic solution to increase indoor micro-environmental conditions to basic [34].

c. Droplet generation rates

Normal oro-nasal activities, like breathing, talking, laughing, singing, and more violent expiratory events, like sneezing and coughing, produce a distribution of respiratory droplet sizes. As we try to retain features of the spread of SARS-CoV-2 we opted to limit the estimate of the droplet generation rates to normal oro-nasal activities. In addition, we neglect super-spreaders, or super-emitters, [37]. The generation rates we analyzed are based on measurements reported by Johnson et al. (2011) [38], see, also, de Oliveira et al. (2021) [31] and Stettler et al. [32]. We used the first two distributions [38], B (bronchiolar droplet generation mode) and L (laryngeal droplet generation mode), to determine the concentration-weighted droplet diameter d_1^{post} . Their emission rate was determined from the reported data for Cn_i , the droplet number concentration (number of droplet per cm^3). The droplet concentration was converted to droplet number per second via the flow rate of the Aerodynamic Particle Sizer (APS) of 5 lt/min. The emitted respiratory droplet per second was converted to number of expelled droplets per day by assuming 1.5 hours of speaking per day (hence the explicit 1.5 in Table I).

Since the APS measures aerosol particles in the size range $0.50 \leq d_p \leq 20$, we decided to use the data of Ref. [38] only for the the smaller diameter d_1^{post} . The emission rate of the d_2^{post} droplets was based on the data of Loudon and Roberts (1967) [39], as described in Ref. [15], and preserving the total volume of the expelled oral fluid.

TABLE I. Simulation parameters: two airborne droplet classes.

Parameter	Description	Estimate	Reference
Biological Parameters			
$\rho_p^{(1)}$	pathogen concentration (d_1^{post})	$7.0 \times 10^7 \text{ \#/cm}^3$ (viral copies / cm^3)	Stadnytskyi et al. (2020) [40]
$\rho_p^{(2)}$	pathogen concentration (d_2^{post})	$3.50 \times 10^6 \text{ \#/cm}^3$ (viral copies / cm^3)	<i>ibid.</i>
μ_I	infection recovery rate	0.1677 (per day)	Kevrekidis et al. (2021) [17]
μ_d	inactivation rate (airborne)	15.13 (per day)	van Doremalen et al. (2020) [41], Buonanno et al. (2020) [1]
p_d	probability of infection (airborne)	0.052 (-)	Drossinos and Stilianakis (2010) [15]
$1/\sigma$	latent period	0.1 or 6 days	Scenario parameter
Behavioural Parameters			
c	contact rate per day	18 #/day	Sypsa et al. (2021) [29]
τ_{d_1}	characteristic breathing time (d_1^{post})	25 min	Based on Drossinos and Stilianakis (2010) [15]
τ_{d_2}	characteristic breathing time (d_2^{post})	1 min	<i>ibid.</i>
Physical and physiological parameters			
d_1^{post}	small-droplet diameter speaking	$2.05 \mu\text{m}$	Johnson et al. (2011) [38]
d_2^{post}	large-droplet diameter speaking	$82.13 \mu\text{m}$	Loudon and Roberts (1967) [39]
ζ_{evap}	evaporation factor	0.40 (-)	Lieber et al. (2021) [42]
B	breathing rate	$12 \text{ m}^3/\text{day}$	Drossinos and Housiadas (2006) [43]
V_{cl}	volume personal cloud	8 m^3	Drossinos and Stilianakis (2010) [15]
q_{d_1}	inhaled-droplet deposition probability (d_1^{post})	0.88 (-)	Drossinos and Housiadas (2010) [43]
q_{d_2}	inhaled-droplet deposition probability (d_2^{post})	1.00 (-)	<i>ibid.</i>
κ_1^d	airborne droplet generation rate speaking (droplets/day) (d_1^{post})	$1.5 \times 51,182 = 76,773 \text{ \#/day}$	Johnson et al. (2011) [38]
κ_2^d	airborne droplet generation rate speaking (droplets/day) (d_2^{post})	$0.8 \times 47,160 = 37,728 \text{ \#/day}$	Loudon and Roberts (1976) [39]
$\lambda_{\text{dep}}^1 = \theta_1$	airborne droplet deposition rate still-air gravitational settling (d_1^{post})	7.8 \#/day	Drossinos and Housiadas (2006) [43]
$\lambda_{\text{dep}}^2 = \theta_2$	settled droplet generation rate still-air gravitational settling (d_2^{post})	$10,558 \text{ \#/day}$	<i>ibid.</i>
λ_{air}	air exchange rate (AER)	4.8 exchanges/day	Buonanno et al. (2020) [1]
Infection-risk parameter			
δt	prediction time	1 or 7 days	estimate

d. Other parameters

All simulation parameters, along with the associated references, are reported in Table I. We note that observations [44] and simulations [16] suggest the importance of the ventilation rate. We chose to use a characteristic value

for typical Italian buildings as reported in Ref. [1], namely $\lambda_{\text{air}} = 0.2$ air exchanges per hour. The evaporation factor ζ_{evap} was chosen to be 0.40, an intermediate value between the recent estimate [42] of 0.20 and our initial estimate [15] of 0.50. The viral inactivation rate in airborne droplets was based on the early measurements of van Doremalen et al. (2020) [41]. It is frequently quoted [1, 2] as the removal rate in terms of the viral half-life $t_{1/2}$ as $\lambda_{\text{inact}} = \ln(2)/t_{1/2}$: both references used $\lambda_{\text{inact}} = 0.63$ per hour gives $\mu_d = 38$ per day. Our estimate is slightly smaller.

-
- [1] G. Buonanno, L. Stabile, and L. Morawska, *Environ. Int.* **141**, 105794. (2020), <https://doi.org/10.1016/j.envint.2020.105794>.
- [2] G. Buonanno, L. Morawska, and L. Stabile, *Environ. Int.* **145**, 106112 (2020), <https://doi.org/10.1016/j.envint.2020.106112>.
- [3] Z. Peng, A. Pineda Rojas, E. Kropff, W. Bahnfleth, G. Buonanno, S. Dancer, J. Kurnitski, M. Li, M. Loomans, L. Marr, L. Morawska, C. Nazaroff, C. Noakes, X. Querol, C. Sekhar, R. Tellier, L. Greenhalgh, L. Bourouiba, A. Boerstra, J. Tang, S. Miller, and J. Jimenez, *Environ. Sci. Technol.* **56**, 1125 (2022), [10.1021/acs.est.1c06531](https://doi.org/10.1021/acs.est.1c06531).
- [4] F. Poydenot, I. Abdourahmane, E. Caplain, S. Der, J. Haiech, A. Jallon, I. Khoutami, A. Loucif, E. Marinov, and B. Andreotti, *PNAS Nexus* **1**, 1 (2022), <https://doi.org/10.1093/pnasnexus/pgac223>.
- [5] B. Jones, P. Sharpe, C. Iddon, E. Abigail Hathway, C. Noakes, and S. Fitzgerald, *Build. Environ.* **191**, 107617 (2021), <https://doi.org/10.1016/j.buildenv.2021.107617>.
- [6] A. Henriques, N. Mounet, L. Aleixo, P. Elson, J. Devine, G. Azzopardi, M. Andreini, M. Rognlien, N. Tarocco, and N. Tang, *Interface Focus* **12**, 20210076 (2022), <https://doi.org/10.1098/rsfs.2021.0076>.
- [7] H. Tang, Z. Pan, and C. Li, *Build. Environ.* **217**, 109067 (2022), <https://doi.org/10.1016/j.buildenv.2022.109067>.
- [8] E. C. Riley, G. Murphy, and R. Riley, *Am. J. Epidemiol.* **107**, 421 (1978), <https://doi.org/10.1093/oxfordjournals.aje.a112560>.
- [9] S. N. Rudnick and D. Milton, *Indoor Air* **13**, 237 (2003), <https://doi.org/10.1034/j.1600-0668.2003.00189.x>.
- [10] C. J. Noakes, C. Beggs, P. Sleight, and K. Kerr, *Epidemiol. Infect.* **134**, 1082 (2006), <https://doi.org/10.1017/S0950268806005875>.
- [11] W. Wells, *Airborne contagion and air hygiene: An ecological study of droplet infections* (Harvard University Press, Cambridge, MA, 1955).
- [12] F. Nordsiek, E. Bodenschatz, and G. Bagheri, *PLoS ONE* **16**, e0248004 (2021), <https://doi.org/10.1371/journal.pone.0248004>.
- [13] R. Riley, *Am. J. Med.* **57**, 466 (1974).
- [14] L. Gammaioni and M. Nucci, *Emerg. Infect. Dis.* **3**, 335–342. (1997), <https://doi.org/10.3201/eid0303.970310>.
- [15] N. Stilianakis and Y. Drossinos, *J. R. Soc. Interface* **7**, 1355 (2010), <https://doi.org/10.1098/rsif.2010.0026>.
- [16] Y. Drossinos, J. Reid, W. Hugentobler, and N. Stilianakis, *Aerosol Sci. Technol.* **56**, 777 (2022), <https://doi.org/10.1080/02786826.2022.2102792>.
- [17] P. G. Kevrekidis, J. Cuevas-Maraver, Y. Drossinos, Z. Rapti, and G. Kevrekidis, *Phys. Rev. E* **104**, 024412 (2021), <https://doi.org/10.1103/PhysRevE.104.024412>.
- [18] J. Cuevas-Maraver, P. Kevrekidis, Q. Chen, G. Kevrekidis, V. Villalobos-Daniel, Z. Rapti, and Y. Drossinos, *Math. Biosci.* **336**, 108590 (2021), <https://doi.org/10.1016/j.mbs.2021.108590>.
- [19] I. Kioutsoukakis and N. Stilianakis, *Int. J. Environ. Res. Public Health* **18**, 1660 (2021), <https://doi.org/10.3390/ijerph18041660>.
- [20] Z. Rapti, J. Cuevas-Maraver, E. Kontou, S. Liu, Y. Drossinos, P. Kevrekidis, M. Barmann, Q.-Y. Chen, and G. Kevrekidis, *Bull. Math. Biol.* **85**, 54 (2023), <https://doi.org/10.1007/s11538-023-01152-5>.
- [21] E. Nardell, *Mycobact. Dis.* **6**, 1000231 (2016), <https://doi.org/10.4172/2161-1068.1000231>.
- [22] C. Beggs, C. Noakes, P. Sleight, L. Fletcher, and K. Siddiqi, *J. Tuberc. Lung Dis.* **7**, 1015 (2003).
- [23] S. G. Wood, J. Craske, and H. C. Burridge, *Sci. Reports* **13**, 17335 (2023), <https://doi.org/10.1038/s41598-023-44527-3>.
- [24] Y. Drossinos, T. Weber, and N. Stilianakis, *Health Sci. Rep.* **4**, e275 (2022), <https://doi.org/10.1002/hsr2.275>.
- [25] M. Bazant and J. Bush, *Proc. Natl. Acad. Sci. U.S.A.* **118**, e2018995118 (2021), <https://doi.org/10.1073/pnas2018995118>.
- [26] P. van den Driessche, *Infect. Dis. Model.* **2**, 288e303 (2027), <http://doi.org/10.1016/j.idm.2017.06.002>.
- [27] M. Robinson, Y. Drossinos, and N. Stilianakis, *Epidemics* **5**, 111 (2013).
- [28] J. Santarpia, V. Herrera, D. Rivera, S. Ratnesar-Shumate, S. Reid, D. Ackerman, P. Denton, J. Martens, Y. Fang, N. Conoan, M. Callahan, J. Lawler, D. Brett-Major, and J. Lowe, *J. Expo. Sci. Environ. Epidemiol.* **32**, 706 (2022), <https://doi.org/10.1038/s41370-021-00376-8>.
- [29] V. Sypsa, S. Roussos, D. Paraskevis, T. Lytras, S. Tsiodras, and A. Hatzakis, *Emerging Infect. Dis.* **27**, 452 (2021), <https://doi.org/10.3201/eid2702.203412>.
- [30] J. Walker, J. Archer, F. Gregson, S. Michel, B. Bzdek, and J. Reid, *ACS Cent. Sci.* **7**, 200 (2021), <https://doi.org/10.1021/acscentsci.0c01522>.
- [31] P. de Oliveira, L. Mesquita, S. Gkantonas, A. Giusti, and E. Mastorakos, *Proc. R. Soc. A* **477**, 20200584 (2021), <https://doi.org/10.1098/rspa.2020.0584>.
- [32] M. Stettler, R. Nishida, P. de Oliveira, L. Mesquita, T. Johnson, E. Galea, A. Grandison, J. Ewer, D. Carruthers, D. David Sykes, and et al., *R. Soc. Open Sci.* **9**, 212022 (2022), <https://doi.org/10.1098/rsos.212022>.

- [33] B. Luo, A. Schaub, I. Glas, L. Klein, S. David, N. Bluvshstein, K. Violaki, G. Motos, M. Pohl, W. Hugentobler, A. Nenes, U. Krieger, S. Stertz, T. Peter, and T. Koh, *Environ. Sci. Technol.* **57**, 486 (2023), <https://doi.org/10.1021/acs.est.2c05777>.
- [34] H. Oswin, A. Haddrell, M. Otero-Fernandez, J. Mann, T. Cogan, T. Hilditch, J. Tian, D. Hardy, D. Hill, A. Finn, A. Davidson, and J. Reid, *Proc. Natl. Acad. Sci. U.S.A.* **119**, e2200109119 (1983), <https://doi.org/10.1073/pnas.2200109119>.
- [35] M. Xenakis, *Entropy* **25**, 896 (2023), <https://doi.org/10.3390/e25060896>.
- [36] M. Robinson, N. Stilianakis, and Y. Drossinos, *J. Theor. Biol.* **297**, 116 (2012), <https://doi.org/10.1016/j.jtbi.2011.12.015>.
- [37] S. Asadi, A. Wexler, C. Cappa, S. Barreda, N. Bouvier, and W. Ristenpart, *Sci. Rep.* **9**, 2348 (2019), <https://doi.org/10.1038/s41598-019-38808-z>.
- [38] G. Johnson, L. Morawska, Z. Ristovski, M. Hargreaves, K. Mengersen, C. Chao, M. Wan, Y. Li, X. Xie, D. Katoshevski, and S. Corbette, *J. Aerosol Sci.* **42**, 839 (2011), <https://doi.org/10.1016/j.jaerosci.2011.07.009>.
- [39] R. Loudon and R. Roberts, *Nature* **213**, 95 (1967), <https://doi.org/10.1038/213095a0>.
- [40] V. Stadnytskyi, C. E. Bax, A. Bax, and P. Anfinrud, *Proc. Natl. Acad. Sci. U.S.A.* **117**, 11875 (2020), <https://doi.org/10.1073/pnas.2006874117>.
- [41] N. Van Doremalen, T. Bushmaker, D. Morris, M. Holbrook, A. Gamble, B. Williamson, A. Tamin, J. Harcourt, N. Thornburg, S. Gerber, J. Lloyd-Smith, E. de Wit, and V. Munster, *N. Engl. J. Med.* **382**, 1564 (2020), <https://doi.org/10.1056/NEJMc2004973>doi:10.1056/NEJMc2004973.
- [42] C. Lieber, S. Melekidis, R. Koch, and H.-J. Bauer, *J. Aerosol Sci.* **154**, 105760 (2021), <https://doi.org/10.1016/j.jaerosci.2021.105760>.
- [43] Y. Drossinos and C. Housidas, in *Multiphase Flow Handbook*, edited by C. T. Crowe (CRC Press, Taylor & Francis Group, Boca Raton, FL, 2006) Chap. 6, pp. 1–58.
- [44] L. Morawska, J. Tang, W. Bahnfleth, M. Bluysen, A. Boerstra, G. Buonanno, G. Cao, S. Dancer, A. Floto, F. Franchimon, and et al., *Environ. Int.* **142**, 105832 (2020), <https://doi.org/10.1016/j.envint.2020.105832>.